IOPscience iopscience.iop.org

Home Search Collections Journals About Contact us My IOPscience

Are the surfaces of CrO_2 metallic?

This article has been downloaded from IOPscience. Please scroll down to see the full text article.

2007 J. Phys.: Condens. Matter 19 315207

(http://iopscience.iop.org/0953-8984/19/31/315207)

View the table of contents for this issue, or go to the journal homepage for more

Download details:
IP Address: 129.252.86.83
The article was downloaded on 28/05/2010 at 19:56

Please note that terms and conditions apply.

J. Phys.: Condens. Matter **19** (2007) 315207 (18pp) doi:10.1088/0953-8984/19/31/315207

Are the surfaces of CrO_2 metallic?

C A Ventrice Jr[1,9], D R Borst[2], H Geisler[3], J van Ek[4], Y B Losovyj[5], P S Robbert[2], U Diebold[6], J A Rodriguez[7], G X Miao[8] and A Gupta[8]

[1] Department of Physics, Texas State University, San Marcos, TX 78666, USA
[2] Department of Physics, University of New Orleans, New Orleans, LA 70148, USA
[3] Institute for Environmental and Industrial Science, Texas State University, San Marcos, TX 78666, USA
[4] Seagate Technology, Bloomington, MN 55435, USA
[5] Center for Advanced Microstructures and Devices, Louisiana State University, Baton Rouge, LA 70806, USA
[6] Department of Physics, Tulane University, New Orleans, LA 70118, USA
[7] Department of Chemistry, Brookhaven National Laboratory 11973, USA
[8] Center for Materials for Information Technology, University of Alabama, Tuscaloosa, AL 35487, USA

E-mail: cventrice@txstate.edu

Received 20 November 2006, in final form 28 January 2007
Published 3 July 2007
Online at stacks.iop.org/JPhysCM/19/315207

Abstract

Previous photoelectron spectroscopy studies of CrO_2 have found either no density of states or a very low density of states at the Fermi level, suggesting that CrO_2 is a semiconductor or a semi-metal. This is in contradiction to calculations that predict that CrO_2 should be a half-metallic ferromagnet. Recently, techniques have been developed to grow high-quality epitaxial films of CrO_2 on TiO_2 substrates by chemical vapour deposition. We present photoelectron spectroscopy measurements of epitaxial $CrO_2(110)/TiO_2(110)$ and $CrO_2(100)/TiO_2(100)$ grown using a CrO_3 precursor. In addition, measurements of epitaxial $Cr_2O_3(0001)/Pt(111)$ films grown by thermal evaporation of Cr in an oxygen atmosphere are presented as a reference for reduced CrO_2 films. The measurements of the CrO_2 surfaces show no emission at the Fermi level after sputtering and annealing the surfaces in oxygen, even though our soft core photoemission data and low-energy electron diffraction measurements provide evidence that stoichiometric CrO_2 is present. The consequence of this is that neither surface of CrO_2 is metallic. This behaviour could result from a metal to semiconductor transition at the (110) and (100) surfaces.

(Some figures in this article are in colour only in the electronic version)

[9] Author to whom any correspondence should be addressed.

 © 2007 IOP Publishing Ltd Printed in the UK

1. Introduction

Chromium dioxide (CrO_2) is a unique ferromagnetic oxide that is predicted to be a half-metallic ferromagnet [1]. Half-metallic ferromagnets are conducting solids whose conduction electrons undergo magnetic ordering with a spin polarization of 100% at 0 K [2]. This unique property occurs when there are charge carriers of only one spin orientation at the Fermi level E_F or when both spin orientations are present but the carriers of one spin orientation are itinerate, whereas the carriers of the opposite spin orientation are localized [3, 4]. The spin polarization of a metallic ferromagnetic material can be defined as

$$P = \frac{N^{\uparrow} - N^{\downarrow}}{N^{\uparrow} + N^{\downarrow}}, \tag{1}$$

where $N^{\uparrow}$ and $N^{\downarrow}$ are the density of states of the spin-up and spin-down electrons at E_F, respectively [5]. Most conventional ferromagnetic materials have a spin polarization of less than 50%. For instance, the spin polarizations of Fe, Co, and Ni measured by superconducting tunnelling spectroscopy give values of 40%, 35%, and 23%, respectively [6]. These elemental ferromagnets have either a partially or fully spin-polarized 3d band. However, the unpolarized 4s band also crosses the Fermi level and contributes enough to the density of states to reduce the spin polarization below 50%.

There are several materials that are predicted to be half-metallic ferromagnets. Most of these materials are metal oxides and include chromium dioxide (CrO_2) [1], magnetite (Fe_3O_4) [7], the mixed valence magnetites ($La_{1-x}A_xMnO_3$; A = Ca, Ba, Sr; $x \sim 0.3$) [8], and the double perovskites (Sr_2FeAO_6; A = Mo, Re) [9]. Of these, chromium dioxide, which is isostructural with SnO_2 and the rutile form of TiO_2, has the simplest crystal structure and has probably been the most thoroughly studied with respect to its predicted half-metallic property [3]. The primary industrial application of chromium dioxide is as a magnetic recording medium for video and audio tapes. Its widespread use in magnetic recording is not a result of its half-metallic property but because it can be grown as a powder composed of needle-like crystallites, which makes it relatively easy to magnetize, and because its Curie temperature is well above room temperature ($T_C \sim 390$ K) [10].

The spin-resolved density of states of CrO_2 calculated using the local spin density approximation (LSDA) of density functional theory (DFT) is shown in figure 1. The details of these calculations are given in a previous publication [11]. As seen in figure 1, the Cr 3d band is exchange split by approximately 2 eV, leaving the majority band partially filled and the minority band completely empty. Using the convention of Coey and Venkatesan [2], CrO_2 is a type I_A half-metal. Half-metallic materials that are predicted to have a completely filled majority band and a partially filled minority band are type I_B half-metals. The calculated spin-resolved density of states presented in figure 1 agrees qualitatively with the results of several other groups that also predict a spin-split band structure of a type I_A half-metal for CrO_2 using either conventional LSDA [1, 11–14], LSDA with the inclusion of a Hubbard parameter U to account for on site Coulombic interactions (LSDA + U) [13, 14], or LSDA with dynamical mean field theory (LSDA + DMFT) [15].

The primary interest in half-metallic ferromagnetic materials is for the development of magnetic sensors and devices with an enhanced performance over those using conventional ferromagnetic materials. One example is the giant magnetoresistance (GMR) spin valve [16], which is a device that consists of two ferromagnetic layers that are separated by a nonmagnetic spacer layer as shown in figure 2. One of the ferromagnetic layers is usually grown on an antiferromagnetic pinning layer, which makes it insensitive to moderate magnetic fields (i.e. a magnetically hard layer). The other layer is usually separated from the first with a conducting

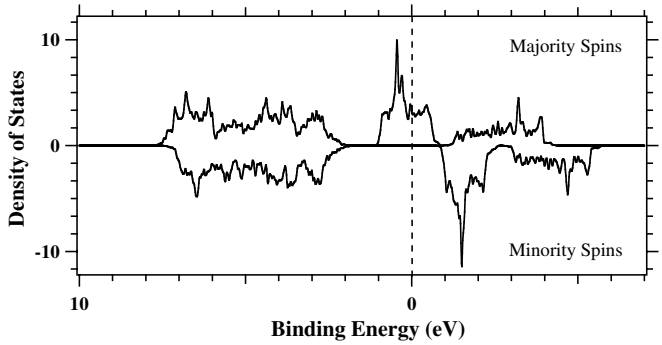

Figure 1. Calculated spin-resolved density of states per eV per formula unit for CrO_2. The majority/minority spin channel is plotted as a positive/negative density of states value.

nonmagnetic layer. This results in a ferromagnetic layer that can switch its magnetization direction with the application of relatively small fields (i.e. a magnetically soft layer). If a current is passed through the device either parallel to the plane (current in plane (CIP) mode) or perpendicular to the plane (current perpendicular to plane (CPP) mode) there will be a change in resistance as the magnetically free layer switches its magnetic orientation relative to the pinned layer. In other words, the electron will normally have a higher probability of scattering as it passes from one magnetic layer to the other in the antiparallel state since it sees a lower density of states in the magnetic layer of opposite polarity. In GMR devices based on conventional ferromagnetic materials such as permalloy, the change in resistance is usually less than 20% at room temperature. If two half-metallic ferromagnetic layers are used instead, changes in resistance of 50% or larger should be possible upon switching from a parallel to an anti-parallel magnetic orientation because of the absence of minority states in the half-metallic ferromagnetic layers.

The development of tunnelling magnetosresistance (TMR) devices based on half-metallic ferromagnetic materials has also received quite a bit of attention recently [17–22]. The main applications of TMR devices are for magnetic field sensors and for magnetoresistive random access memory (MRAM). The TMR and GMR devices have a similar construction, except that the nonmagnetic spacer layer is replaced with an insulating barrier that is thin enough (∼2 nm) for a measurable quantum mechanical tunnelling current to be detected. A schematic of a TMR device is shown in figure 3. When a bias is applied between the two ferromagnetic layers, electrons will tunnel from one layer to the other through the insulating intralayer. As the free magnetic layer switches from the parallel to the antiparallel magnetization orientation, there will be a drop in the tunnelling current since the electrons are now being injected into minority states instead of majority states. A simple model for spin polarized tunnelling which neglects spin-flip scattering at the interfaces or within the insulating layer was developed by Julliére in 1975 [23] and is given by

$$\mathrm{TMR} = \frac{2P_1P_2}{1 - P_1P_2}. \tag{2}$$

This model relates the TMR effect to the spin polarization P in each ferromagnetic layer. Using conventional ferromagnetic layers with an AlO_x barrier, TMR of ∼50% has been recorded [24]. If the conventional ferromagnetic layers are replaced with half-metallic ferromagnetic layers, the tunnelling current should go to zero as the two layers switch from a parallel to an antiparallel magnetic orientation (i.e. an infinite TMR effect) if there is no spin-flip scattering in the films

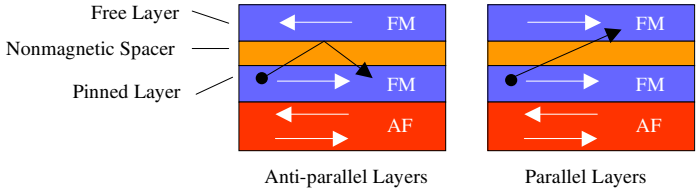

Figure 2. Schematic of a GMR device. As majority-spin electrons pass from one ferromagnetic material to the other, they will normally have a higher probability of scattering in the anti-parallel configuration since the transport is into the minority states of the second ferromagnet.

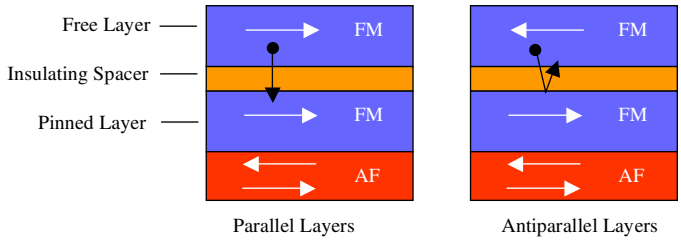

Figure 3. Schematic of a TMR device. For two ferromagnetic electrodes with a parallel magnetic alignment, majority-spin electrons can access majority-spin states on the other side of the insulating spacer, resulting in a tunnel current if a bias V is applied between the electrodes. If the magnetic orientation of the free layer is switched to the antiparallel alignment, a drop in tunnel current is expected to occur since the density of states available for majority-spin transport will be reduced.

or at the interfaces. This predicted very low quiescent current in the antiparallel state is the primary reason for the interest in using half-metallic materials in MRAM applications.

Although the performance of devices based on half-metallic ferromagnetic materials is predicted to be superior to those based on conventional ferromagnetic materials, in almost all published studies where one or more of the ferromagnetic electrodes was replaced with a half-metallic ferromagnet, the performance was degraded instead of enhanced [17–22, 25–27]. Various reasons have been given for the poor performance of devices that are based on half-metallic ferromagnetic materials. One of the most obvious reasons is spin-flip scattering during the transport process, which can be caused by interfacial roughness or from disorder within the ferromagnetic electrodes or in the nonmagnetic spacer layers. The stoichiometry of the half-metallic material at its surface or interface can also be an issue. For instance, the rutile structured CrO_2 will reduce to the corundum structured Cr_2O_3 at temperatures above $\sim$400 °C at atmospheric pressure [28]. Therefore, it is generally accepted that a Cr_2O_3 surface layer can form under vacuum processing conditions at elevated temperatures [29–33]. Ideally, devices based on heteroepitaxial layers with a low lattice mismatch should be largely free of nonstoichiometries and have a relatively low defect density. An advancement towards this goal was recently achieved by Miao *et al* [27]. In this study, heteroepitaxial bilayers of CrO_2/SnO_2 were grown on $TiO_2(100)$ substrates by chemical vapour deposition (CVD). Deposition of Co on the insulating SnO_2 layers resulted in the formation of TMR devices after patterning. The resistance as a function of applied magnetic field at 10 K for a device with a 1.7 nm SnO_2 barrier gave the maximum TMR value of only 14%. By assuming an effective spin polarization of 35% for the Co overlayer, the maximum observed TMR value results in a spin polarization of only 19% for the CrO_2 layer [27].

Since the actual performance of devices based on materials that are predicted to be half-metallic ferromagnets is almost always worse than those based on conventional ferromagnetic

materials, one must ask the question: *Is there any direct experimental evidence of half-metallicity for any of the materials predicted to be half-metallic ferromagnets?* To be a half-metallic ferromagnet, a material must be a metal and have and a spin polarization of 100% at the Fermi level. In this article, the issue of whether or not the surfaces of CrO_2 are half-metallic is addressed. Methods of measuring this property will be described, and a review of previous experimental results and our recent photoelectron spectroscopy results on epitaxial CrO_2 films will be presented.

2. Measurement of half-metallicity in ferromagnetic materials

Ideally, one would like to perform an experiment where the density of states and spin polarization at the Fermi level (E_F) could be measured simultaneously with the electrical conductivity of the material to confirm directly that it is a half-metallic ferromagnetic material. In practice, the electrical conductivity is measured separately from the spin polarization and the density of states at E_F. Experimental techniques that can be used to determine the spin polarization include spin-resolved ultra-violet photoelectron spectroscopy (SP-UPS) [34] and various transport measurement experiments using point contacts or tunnelling junctions either between two ferromagnetic electrodes or one ferromagnetic and one superconducting electrode [3]. To determine if a material is a metal, a combination of experimental techniques is needed. Ultra-violet photoelectron spectroscopy (UPS) measurements can be used to determine the occupied density of states [34, 35], inverse-photoelectron spectroscopy measurements can be used to determine the unoccupied density of states [34], and temperature-dependent resistivity measurements show whether the material is a conductor or an insulator [36]. For instance, if the resistivity of a material decreases as its temperature approaches 0 K, the material is a conductor, but this does not uniquely determine whether the material is a metal or a semi-metal. In semi-metals, the density of states of an energy band just crosses E_F either from the conduction band or valence band side [37]. This results in a resistivity that decreases with decreasing temperature; however, the low density of states at E_F for semi-metals results in resistivities that are typically an order of magnitude or more higher than for metals. To determine whether a material with a low conductivity is just a metal with a high defect density or a semi-metal, both photoelectron spectroscopy and inverse-photoelectron spectroscopy measurements are needed to determine the density of states both below and above E_F.

2.1. Electrical conductivity

Early measurements of the electrical conductivity of CrO_2 provide conflicting values, probably due to differences in sample purity and because these measurements were performed on compacted powders [28]. Although large single crystals of CrO_2 are not available, techniques have been developed to grow high-quality epitaxial films on TiO_2 substrates by CVD [38–42]. Measurements of the resistivity of CrO_2 epitaxial films as a function of temperature show a continuous drop in resistivity as the temperature approaches 0 K, which indicates that CrO_2 is a conductor [38–44]. For instance, Gupta *et al* [44] have measured a room temperature resistivity of 230 $\mu\Omega$ cm that drops to 2 $\mu\Omega$ cm at 5 K for transport along the *c*-axis of epitaxial $CrO_2(100)$ films grown on $TiO_2(100)$. A comparison of resistivities of Cu (an s-metal), Fe (a ferromagnetic d-metal with partial s character), Bi (a semi-metal), and CrO_2 at 273 and 77 K are shown in table 1.

At 273 K, CrO_2 is a rather poor conductor. This is a general characteristic of most conducting oxides and is attributed to the large cross section for scattering of conduction electrons with optical-phonons and other collective excitations in the oxide. At 77 K, the resistivity of CrO_2 drops to about a fifth of the resistivity of Bi, but it is still an order of

Table 1. Resistivities in $\mu\Omega$ cm of various conductors at 273 and 77 K.

	ρ (273 K)	ρ (77 K)
Cu [45]	1.6	0.2
Fe [45]	8.9	0.7
Bi [45]	107	35
CrO_2 [44]	200	7

magnitude greater than that of Fe at that temperature. The resistivity values in table 1 for CrO_2 are for epitaxial films. Because of lattice mismatch with the TiO_2 substrate, dislocations will be present in the films; therefore, the measured value of 7 $\mu\Omega$ cm is probably an upper limit to CrO_2's resistivity at 77 K.

2.2. Spin polarization measured by Andreev reflection

Interpreting spin polarization values measured by transport through a magnetic tunnel junction or across a superconductor/ferromagnetic interface is complicated by scattering processes that can occur at the interfaces or the intralayers of the junction [4]. In addition, point contact techniques such as Andreev reflection [46], which is performed by making direct contact between a superconducting tip and the surface of the substrate, can result in damage to the crystal structure at the tip–surface interface and may affect the local electronic and magnetic structure. For some transport measurement techniques, an enhanced polarization may be measured if multiple reflections occur within the barrier. Spin polarizations of CrO_2 using the point-contact Andreev reflection technique have ranged from 81% [41] to 98% [42]. Variations in the measured values of the spin polarization using this technique probably depend on the sample growth techniques and differences in the sample–tip interaction. It is important to note that this technique provides a spin polarization of electrons within a few meV of the Fermi level, which is the energy range that governs the transport properties in devices. However, this technique provides little information about the magnitude of the density of states at E_F, which also affects the material's transport properties.

2.3. Spin-polarized photoelectron spectroscopy

The most direct measurement of spin polarization is from SP-UPS. Photoemission spectra can be measured with photons from either a gas discharge lamp or a synchrotron light source and are almost always performed under ultra-high vacuum (UHV) conditions. This technique is a photon-in/electron-out process. The kinetic energy KE of the photoelectrons excited by an incident photon of energy $h\nu$ is given by

$$\mathrm{KE} = h\nu - e\phi - E_B, \tag{3}$$

where ϕ is the work function of the spectrometer and E_B is the binding energy of the electron measured with respect to E_F [35]. By placing a Mott spin polarimeter at the collector of the electron spectrometer, spin-resolved photoemission spectra can be measured [47]. The kinetic energies of the photoelectrons in a UPS experiment typically range from about 15 to 100 eV. Since the mean free path of electrons in matter is $\sim$10 Å in this energy range, this is an extremely surface sensitive technique. Therefore, the electronic and magnetic properties measured with spin-resolved UPS are from the outermost atomic layers of the crystal, which may differ from the bulk properties. Since CrO_2 can reduce to Cr_2O_3 under vacuum conditions at elevated temperatures, it is also important to monitor the structure of the surface with low energy electron diffraction (LEED) or scanning tunnelling microscopy (STM) to ensure that the surface has not converted to Cr_2O_3. Another factor that must be considered with UPS

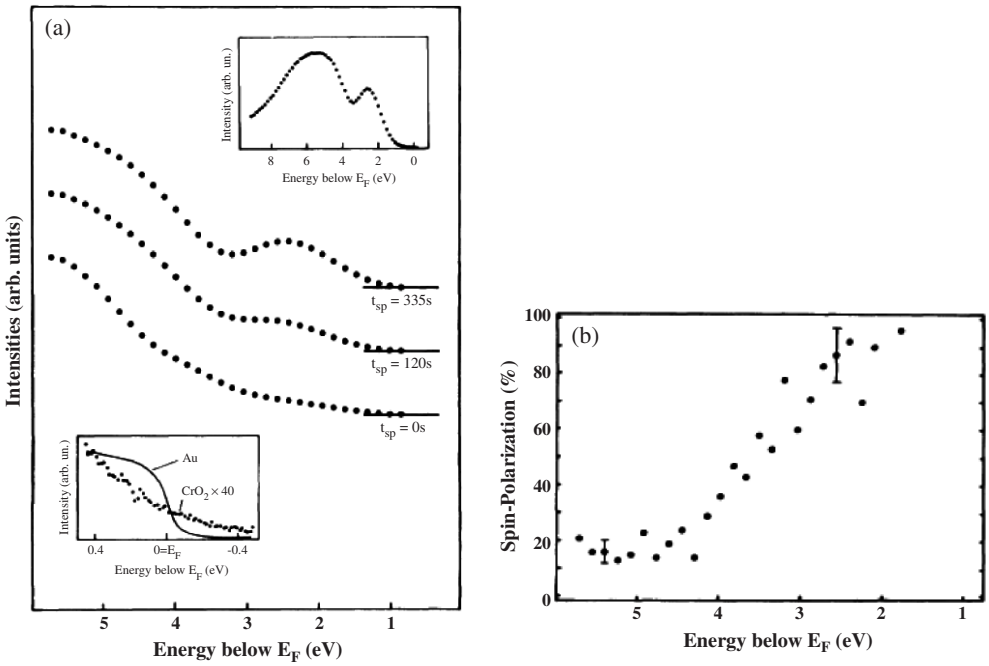

Figure 4. (a) Photoelectron spectra of polycrystalline CrO_2 films measured at 300 K with $h\nu = 21.2$ eV for different sputtering times (t_{sp}) with 500 eV Ne ions. Upper inset shows the larger binding energy scale for a spectrum after 335 s of sputter cleaning. Lower inset shows comparison between polycrystalline Au foil and CrO_2 spectra (expanded by a factor of 40) in the vicinity of the Fermi level. (b) Spin polarization of photoelectrons after 120 s of sputter cleaning. Used with permission from [49].

experiments is the instrumental energy resolution. The resolution will depend on the type of light source, the energy of the photons, the kinetic energy of the photoelectrons, and the type, size, and pass energy of the electron analyser. Although an instrumental resolution of <5 meV is possible with UPS [48], the typical instrumental resolution (photon + electron) for synchrotron-based UPS measurements at photon energies below 100 eV is 50–150 meV with a 150 mm radius hemispherical analyser [34, 35].

Approximately a year after the original paper by Schwarz [1] was published that predicted half-metallicity in CrO_2, Kämper *et al* published SP-UPS measurements for polycrystalline CrO_2 films [49]. These films were grown by thermal decomposition of CrO_3 in a closed reactor onto heated substrates of RuO_2, TiO_2, or Al_2O_3. For CrO_2 films inserted into their UHV chamber without any surface preparation, the UPS spectra show very little emission in the valence region up to a binding energy of $\sim$3 eV, as seen in figure 4(a). Sputtering of the surface with 500 eV Ne ions resulted in an increase in emission in the range of binding energies from 1 to 3 eV with a spin polarization of $\sim$90% over that energy range (figure 4(b)). Annealing the films in UHV at 200 °C for 12 h resulted in a shift of the valence features by $\sim$1 eV to lower binding energy and a loss of spin polarization. Their interpretation of these results was that sputtering created a clean CrO_2 surface and that subsequent annealing in UHV reduced the surface to Cr_2O_3. If this interpretation is correct, the very low emission up to 1 eV below the Fermi level and the lack of a change in inflection of intensity at E_F provide evidence that the surface of these polycrystalline CrO_2 films is not metallic.

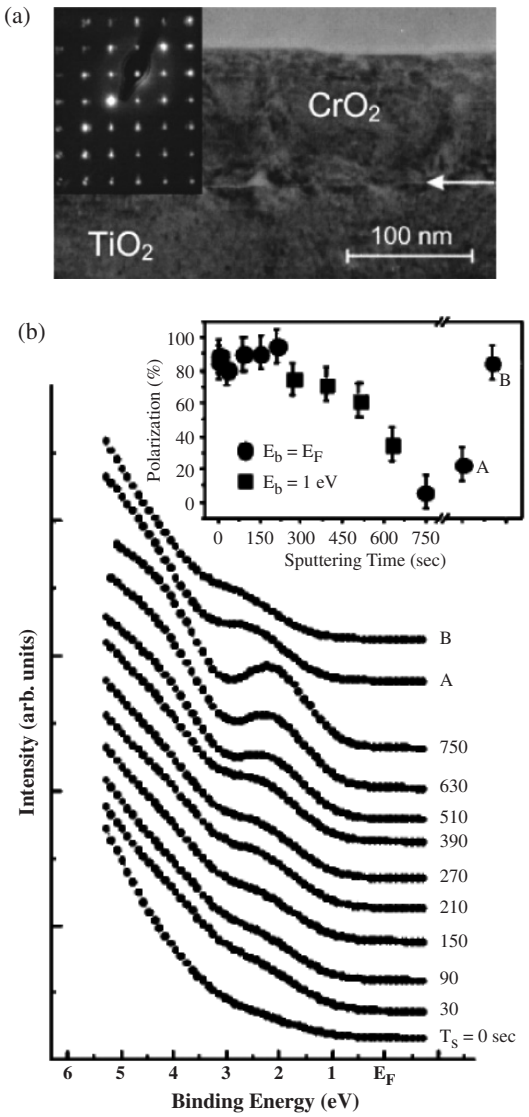

Figure 5. (a) $CrO_2(100)$ film grown on a $TiO_2(100)$ substrate. In the TEM cross section image the white arrow indicates a sharp interface between the $CrO_2(100)$ film and the $TiO_2(100)$ substrate. Inset shows an electron diffraction pattern of a $CrO_2(100)$ film on a $TiO_2(100)$ substrate with the incident e-beam parallel to the [001] direction of $CrO_2(100)$. (b) Photoelectron spectra of a $CrO_2(100)$ film ($h\nu = 21.2$ eV) as a function of binding energy (lower part) and the resulting spin polarization (upper part) for different sputtering times. Solid circles indicate spin polarization at the Fermi level and solid squares at 1 eV binding energy. After 750 s sputtering time $CrO_2(100)$ film was annealed at 100 °C (A) and 150 °C (B) for 12 h each, respectively. Used with permission from [50].

A SP-UPS study of epitaxial $CrO_2(100)$ films grown on $TiO_2(100)$ by Dedkov *et al* [50] provides results that also show high values for spin polarization (80%–95%) and very low valence emission up to 1 eV below E_F. Transmission electron microscopy (TEM) images show an abrupt interface, and high-energy electron diffraction images indicate that the films are single-crystal $CrO_2(100)$, as shown in figure 5(a). As with the previous study, very little

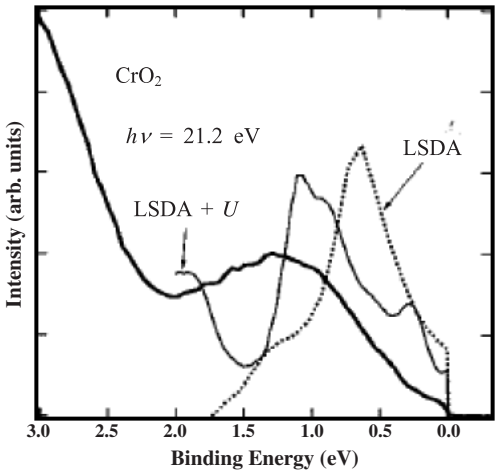

Figure 6. High-resolution photoelectron spectrum of CrO_2 ($h\nu = 21.2$ eV, $\Delta E \sim 25$ meV) compared with bandstructure calculations using LSDA and LSDA+U. Used with permission from [51].

valence emission is observed for the as-grown samples (figure 5(b)). Sputtering with 500 eV Ar ions produced a rise in the valence features for binding energies less than 3 eV. The spin polarization of the photoelectrons near the Fermi level was observed to be greater than 80% for sputter times less than 300 s. After 750 s of sputtering, most of the spin polarization was lost, and a low-temperature anneal at 150 °C for 12 h was necessary to return the spin polarization to levels above 80%. It was presumed that the low-temperature anneal healed surface disorder induced by sputtering. However, no LEED results were presented to confirm the presence of an ordered $CrO_2(100)$ surface after the anneal.

2.4. Conventional photoelectron spectroscopy

Conventional UPS measurements provide a measure of the total occupied density of states of the surface (i.e. a sum of the spin-up and spin-down photoemission intensities). To the best of our knowledge, the only UPS study of CrO_2 that shows a non-zero intensity at E_F was by Tsujioka *et al* [51]. Their samples were prepared by sintering CrO_2 powders under 6 GPa of O_2 to form polycrystalline pellets. The surface of the samples was cleaned *in situ* by scraping with a diamond file. As can be seen in figure 6, there is a finite photoemission intensity and a slight change in the slope of the photoemission intensity plot as the Fermi level is crossed in the UPS spectra. In addition, the peak of the Cr 3d valence emission is ∼1.3 eV below E_F, which is ∼1 eV lower in binding energy than the value measured in the spin-resolved UPS studies where the surfaces were prepared by sputtering [49, 50]. The measured photoelectron emission just below E_F is less than 10% of the maximum of the 3d emission, which is much smaller than the values predicted by the LSDA or LSDA + U calculations (28% and 23%, respectively). The most likely reason for the shift in 3d emission of ∼1 eV towards E_F when compared to other UPS studies of CrO_2 is the unique surface preparation technique. Mechanical scraping will result in considerable surface roughness and may also result in a non-uniform surface cleanliness, whereas sputtering is expected to cause more structural damage at the microscopic level. Therefore, it is unclear which surface preparation technique is providing a true picture of the electronic properties of CrO_2.

The only previously published photoelectron spectroscopy study where the surface structure of CrO_2 has been identified was a recent study by Dedkov *et al* [52]. Epitaxial $CrO_2(100)$ films were grown on $TiO_2(100)$ substrates by thermal evaporation of CrO_3. LEED was performed on their samples immediately after insertion into their UHV chamber and

showed a rectangular diffraction pattern with the correct lattice parameters for the (100) surface. STM measurements revealed flat terraces on the surface with step heights of 4.4 Å, which is consistent with the expected step height of $CrO_2(100)$. Valence band photoelectron spectroscopy spectra were measured from these surfaces and show emission at E_F. However, the spectra were taken on a soft x-ray beamline with photon energies of 575 eV and higher and do not have sufficient resolution to determine the density of states near E_F.[10] It is noted that the peak in the 3d emission is observed to be 2 eV below E_F, which is similar to the previous study of $CrO_2(100)$ that used sputtering for surface cleaning [50].

2.5. Summary of previous results for CrO_2

Both Andreev reflection measurements and spin-resolved photoemission measurements provide evidence for high spin polarization of the valence electrons of CrO_2. On the other hand, the relatively low conductivity of CrO_2 and the low photoemission intensity for energies up to 1 eV below E_F measured in previous UPS studies seem to indicate that CrO_2 behaves more like a semi-metal than a metal. Since Cr_2O_3 is an anti-ferromagnetic, semiconducting oxide with a band gap of $\sim$1.7 eV [53], the lack of photoemission intensity for binding energies just below E_F could also be the result of a thin surface layer of Cr_2O_3. However, this does not explain the high degree of spin polarization measured in the SP-UPS experiments. Although a net polarization can be induced in a thin Cr_2O_3 overlayer by the underlying CrO_2 [31, 32], spin polarizations greater than 90% are not very likely. Therefore, it is still an open question as to whether the low density of states measured near the Fermi level with UPS is an intrinsic property of CrO_2 and/or its surfaces or if this results from problems with the stoichiometry of the CrO_2 surface.

3. Photoelectron spectroscopy measurements of $CrO_2(100)/TiO_2(100)$ and $CrO_2(110)/TiO_2(110)$

To better understand the electronic structure of CrO_2, we have performed angle-resolved UPS measurements of epitaxial films of $CrO_2(100)/TiO_2(100)$ and $CrO_2(110)/TiO_2(110)$ at the Center for Advanced Microstructures and Devices (CAMD) synchrotron in Baton Rouge, Louisiana. Because the formation of Cr_2O_3 at the surface of CrO_2 is possible under UHV conditions, these data were compared with valence band and soft core (Cr 3p and O 2s) photoemission spectra of epitaxial $Cr_2O_3(0001)/Pt(111)$, which were measured at the National Synchrotron Light Source (NSLS) at Brookhaven National Laboratory and are used in this study as a reference for the electronic structure of Cr_2O_3. To monitor the crystal structure of the surface region, LEED measurements have been performed during various stages of the surface preparation procedure.

3.1. Experimental procedure

The epitaxial CrO_2 films were grown on TiO_2 substrates at the Center for Materials for Information Technology at the University of Alabama using a CrO_3 precursor. The details of the growth procedure have been previously published [39]. The samples were shipped in a desiccator to the CAMD synchrotron where UPS and LEED measurements were performed. Both CrO_2 and TiO_2 crystallize in the tetragonal rutile structure. The lattice constants of CrO_2 are $a_0 = 4.42$ Å and $c_0 = 2.92$ Å and of TiO_2 are $a_0 = 4.59$ Å and $c_0 = 2.96$ Å [54], which

[10] Emission is observed at $\sim$1 eV *above* the Fermi level in the spectra presented in figure 3 of [52], which means that their instrumental resolution is no better than $\sim$1 eV.

Table 2. Surface lattice constants of CrO_2 and Cr_2O_3.

	a_s (Å)	b_s (Å)	Symmetry
$CrO_2(100)$	4.42	2.92	Rectangular
$CrO_2(110)$	6.25	2.92	Rectangular
$CrO_2(001)$	4.42	4.42	Square
$Cr_2O_3(0001)$	4.95	4.95	Hexagonal

results in a lattice mismatch of -4% in the [100] direction and -1% in the [001] direction. The (100), (110), and (001) surfaces of TiO_2 are all non-polar; however, the (110) surface, which has the lowest number of dangling bonds per unit area, is the most stable [55, 56]. The (001) surface is the least stable of the three and tends to facet or reconstruct. Therefore, only epitaxial CrO_2 films grown on the $TiO_2(100)$ and $TiO_2(110)$ surfaces were used in this study. The approximate thickness of the films grown on each substrate was 150 nm.

The UPS measurements of the CrO_2 films were carried out using synchrotron radiation, dispersed by a 3 m toroidal grating monochromator (3m-TGM) at CAMD. The endstation has conventional surface preparation and analysis instrumentation including a sputter gun, O_2 source, LEED optics, and 50 mm hemispherical analyser with $\pm 1^\circ$ angular acceptance mounted on a two-axis goniometer for angle-resolved UPS measurements [57]. The base pressure of the endstation is 1×10^{-10} Torr, and it has a load lock for insertion of samples into the analysis chamber without breaking UHV. All measurements were made using the high-energy grating, which has a usable photon flux from 40 to 160 eV. The instrumental resolution for the UPS measurements was estimated to be $\sim$200 meV by measuring the half-width of the Fermi cutoff of a clean Pt(111) crystal at a photon energy of 75 eV and subtracting the thermal spread of the Fermi function at 300 K (half width of 1.76 kT = 46 meV). The CrO_2/TiO_2 crystals were 5 mm $\times$ 5 mm in size and mounted on a molybdenum plate with spot welded tantalum wires. The sample stage consists of a stainless steel tube for liquid nitrogen cooling with a copper block at the end where the molybdenum sample plate is inserted. Since a thermocouple is not attached directly to the sample plate or the sample itself, the anneal temperatures of the samples are estimated to be accurate to only $\pm 100\,^\circ$C. The LEED optics at the 3m-TGM endstation is a front-view, four-grid system. The surface lattice constants, a_s and b_s, of the non-polar surfaces of CrO_2 and Cr_2O_3 are given in table 2. For the $CrO_2(100)$ and $CrO_2(110)$ surfaces, rectangular LEED patterns should be observed with a reciprocal lattice ratio of 1.5 and 2.1, respectively. The most stable surface of Cr_2O_3 is the non-polar (0001) surface, which has a hexagonal symmetry.

The UPS measurements of the epitaxial $Cr_2O_3(0001)/Pt(111)$ films were performed on the U4A beamline at the NSLS. The films were grown *in situ* by evaporating Cr in an O_2 atmosphere of 2×10^{-6} Torr onto a Pt(111) crystal at $300\,^\circ$C. The U4A beamline is equipped with a 6m-TGM, and the endstation has a fixed 150 mm hemispherical analyser. The instrumental resolution for the UPS measurements at U4A was estimated to be $\sim$75 meV using the same technique that was used for the CAMD data. Further details of the endstation and sample preparation conditions are given in a previous publication [11].

3.2. UPS and LEED measurements

Upon insertion of each $CrO_2(100)$ and $CrO_2(110)$ sample into the analysis chamber at CAMD, LEED measurements were performed, but no diffraction spots were observed for any of the as-inserted samples. Valence band UPS spectra taken at 50 eV photon energy for the $CrO_2(100)$ and $CrO_2(110)$ surfaces immediately after insertion into the analysis chamber are shown in

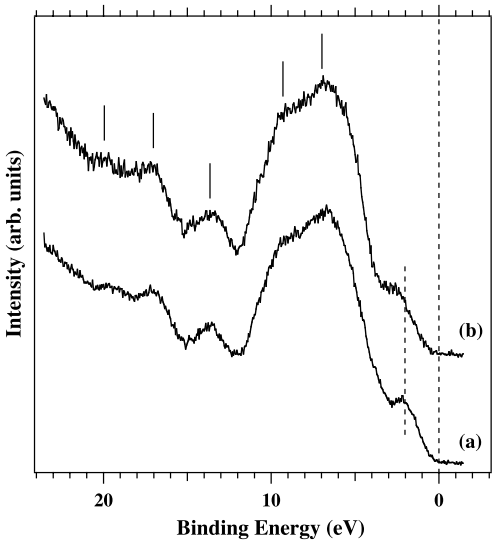

Figure 7. Valence band photoelectron spectra measured at $h\nu = 50$ eV and normal emission of (a) as-inserted $CrO_2(100)/TiO_2(100)$ sample and (b) as-inserted $CrO_2(110)/TiO_2(110)$ sample. Peak positions of surface contaminates are marked with solid ticks.

figure 7. A series of peaks in the spectra ranging from 7 to 20 eV binding energy are observed that are a signature of surface contaminants. Peaks in the range of 7–15 eV are most likely from hydroxyl groups and H_2O adsorbed on the surface [58], which is expected for an oxide exposed to air. The peaks at higher binding energies are probably from hydrocarbons adsorbed on the surface. As expected with a sample with surface contamination, the Cr 3d emission at ∼2 eV is suppressed, and there is no signature of a Fermi edge. Attempts were made to clean the surface with a mild anneal at ∼200 °C in an oxygen atmosphere of 1×10^{-6} Torr, but only a slight increase in the Cr 3d emission was observed. Sputtering of the surface was necessary to completely remove the surface contamination layer.

A series of valence spectra for the $CrO_2(110)$ surface are displayed in figure 8 and show the effect that sputtering and annealing of the crystal in O_2 has on the surface. The clean Pt(111) spectrum is shown in the figure to establish the position of the Fermi level. After 10 min of sputtering with 500 eV Ar ions, there is a large increase in the valence emission, and the peak position of the 3d emission is observed at 2.0 eV below E_F. Annealing the crystal at ∼200 °C in 1×10^{-6} Torr of O_2 for 10 min followed by a 10 min cool down in O_2 results in almost no change from the spectrum from the sputtered sample. Repeating the annealing procedure at ∼400 °C results in a shift of the 3d peak by 0.15 eV towards E_F. None of the $CrO_2(110)$ spectra show emission at E_F. A reference spectrum for $Cr_2O_3(0001)$ is also shown in this figure, and its features are similar to the $CrO_2(110)$ spectra. The main difference between these spectra is the ratio of the valence emission from the 3d states to the emission in the range of 3–9 eV, which is primarily from the O 2p states. This ratio is higher for Cr_2O_3.

The soft core emissions for the $CrO_2(100)$ surface taken at a photon energy of 120 eV are shown in figure 9. As expected for a sample with surface contamination, the Cr 3p and O 2s emissions are almost completely attenuated for the as-inserted sample. After sputtering the sample, the Cr 3p and O 2s cores appear. Annealing the sample in O_2 causes no visible shifts in either the Cr 3p or O 2s core peaks. Some emission from the Ta wire is also observed in the spectra, which is from the mounting wire. A spectrum for Cr_2O_3 taken at a photon energy of 155 eV is also shown. This spectrum shows a higher Cr to O peak ratio than for the CrO_2 spectra. However, the spectra for the two samples were taken at two different photon energies, so the energy dependence of the photoemission cross sections for the Cr 3p and

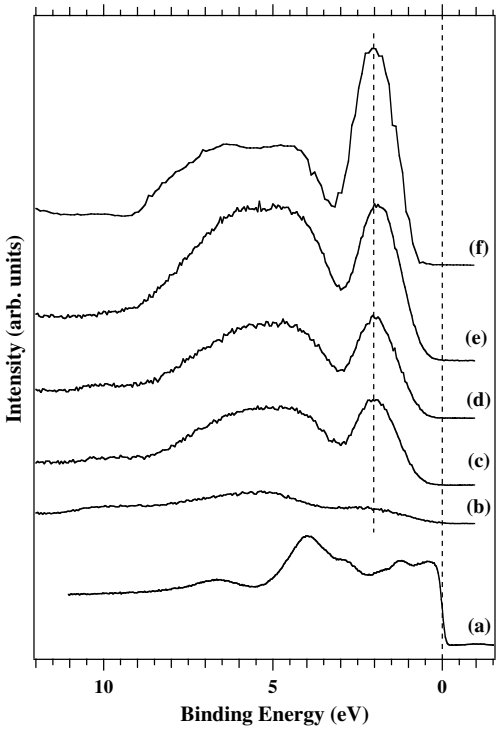

Figure 8. Valence band photoelectron spectra measured at $h\nu = 75$ eV and normal emission of (a) clean Pt(111) crystal, (b) as-inserted $CrO_2(110)/TiO_2(110)$ sample, (c) sample sputtered for 10 min with 500 eV Ar ions, (d) sample annealed at 200 °C in 1×10^{-6} Torr O_2, (e) sample annealed at 400 °C in 1×10^{-6} Torr O_2, and for comparison (f) $Cr_2O_3(0001)/Pt(111)$.

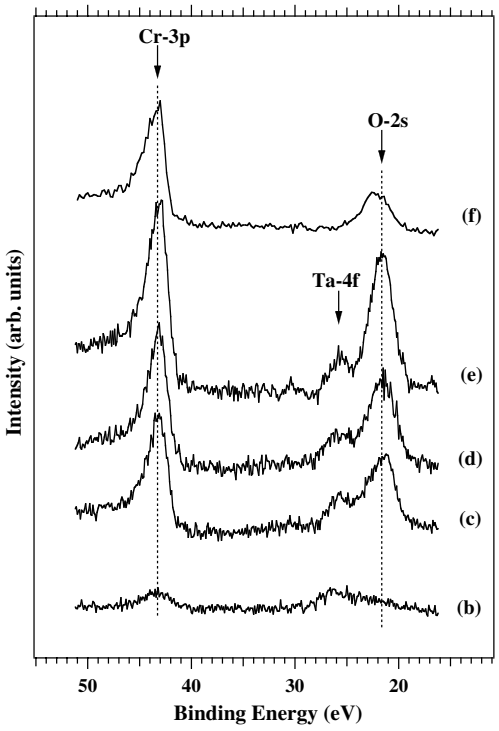

Figure 9. Cr 3p and O 2s core-electron spectra measured at $h\nu = 120$ eV and normal emission of (b) as-inserted $CrO_2(110)/TiO_2(110)$ sample, (c) sample sputtered for 10 min with 500 eV Ar ions, (d) sample annealed at 200 °C in 1×10^{-6} Torr O_2, (e) sample annealed at 400 °C in 1×10^{-6} Torr O_2, and for comparison (f) $Cr_2O_3(0001)/Pt(111)$ measured at $h\nu = 155$ eV.

Table 3. Photoemission cross sections for Cr 3p and O 2s [59].

$h\nu$ (eV)	$\sigma_{\text{O 2s}}$ (Mb)	$\sigma_{\text{Cr 3p}}$ (Mb)
120	0.42	1.07
155	0.29	1.04

O 2s cores must be taken into account when comparing the peak ratios of the two different samples. These photoemission cross sections are compiled in table 3. A detailed analysis of the core ratios is presented in section 4. After the final anneal at ∼400 °C in O_2, LEED was measured, and a rectangular diffraction pattern with the correct symmetry for the $CrO_2(110)$ surface was observed. However, the diffraction spots were quite broad, and there was a high diffuse background intensity, indicating that there is a lot of disorder at the surface.

A series of valence band UPS spectra for the $CrO_2(100)$ surface is shown in figure 10. The spectrum of the as-inserted $CrO_2(100)$ surface exhibits a large attenuation of the valence features, similar to what was observed for the $CrO_2(110)$ surface. Sputtering the surface results in a rise in the valence emission and a shift of the 3d peak to 2.5 eV below E_F. Annealing the crystal at ∼400 °C in 1×10^{-6} Torr of O_2 for 10 min followed by a 10 min cool down in O_2 results in a shift in the peak of the 3d emission to 1.9 eV. As with the $CrO_2(110)$ samples, none of the spectra from $CrO_2(100)$ show emission at E_F.

The soft core emissions for the $CrO_2(100)$ surface are shown in figure 11. For the as-inserted sample, the Cr 3p and O 2s emissions are almost completely attenuated. Interestingly, both the Cr 3p and O 2s peaks of the sputtered surface are shifted by ∼0.5 eV to higher binding energy with respect to the peaks after the oxygen anneal. The shift in both of the core peaks and the valence features after sputtering is a signature of sample charging, which should not occur for a conducting sample.

4. Discussion

The central question that we would like to answer in this study is whether the electronic structure of CrO_2 is that of a metal or of a semi-metal. However, our measurements are only sensitive to the first ∼10 Å of the epitaxial films, so the electronic structure of the surface region of our samples is what is revealed, not the bulk properties. None of the valence band photoelectron spectra for $CrO_2(110)$ or $CrO_2(100)$ presented in this study show emission at E_F, which is consistent with either a semiconducting behaviour or a semi-metallic behaviour with an energy band crossing E_F from the conduction band side. Since diffraction patterns with a rectangular symmetry were observed with LEED after annealing the epitaxial films in oxygen, some fraction of the surface region of the crystals should be ordered CrO_2. Therefore, emission at E_F is expected if the surfaces of CrO_2 are metallic since LEED and UPS have similar probe depths. On the other hand, it is almost certain that some portion of the epitaxial film is reduced to Cr_2O_3 after sputtering or annealing in oxygen. Although no LEED patterns with a hexagonal symmetry were observed, which would be a signature of the non-polar (0001) surface of Cr_2O_3, there could be either disordered patches of Cr_2O_3 coexisting with CrO_2 on the surface or a very thin layer of disordered Cr_2O_3 layer on top of the CrO_2.

An estimate of the fraction of the surface region reduced to Cr_2O_3 can be obtained by analysing the O 2s to Cr 3p core ratios. Unfortunately, the overlap of the Ta-4f peak with the O 2s peak in figures 9 and 11 makes it difficult to accurately determine the area under the O 2s core. As a first-order approximation for the ratio of the areas under the O 2s and Cr 3p cores, the ratio of the peak heights measured after subtracting a linear background is used (i.e. $A_O/A_{Cr} \approx H_O/H_{Cr}$). An estimate of the surface stoichimetry can be obtained by multiplying the core ratios by the ratio of the Cr 3p to O 2s photoemission cross sections at

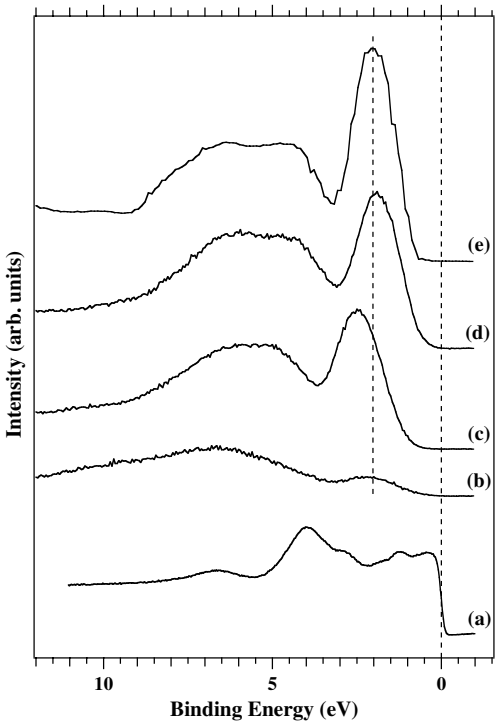

Figure 10. Valence band photoelectron spectra measured at $h\nu = 75$ eV and normal emission of (a) clean Pt(111) crystal, (b) as-inserted $CrO_2(100)/TiO_2(100)$ sample, (c) sample sputtered for 10 min with 500 eV Ar ions, (d) sample annealed at $\sim$400 °C in 1×10^{-6} Torr O_2, and for comparison (e) $Cr_2O_3(0001)/Pt(111)$.

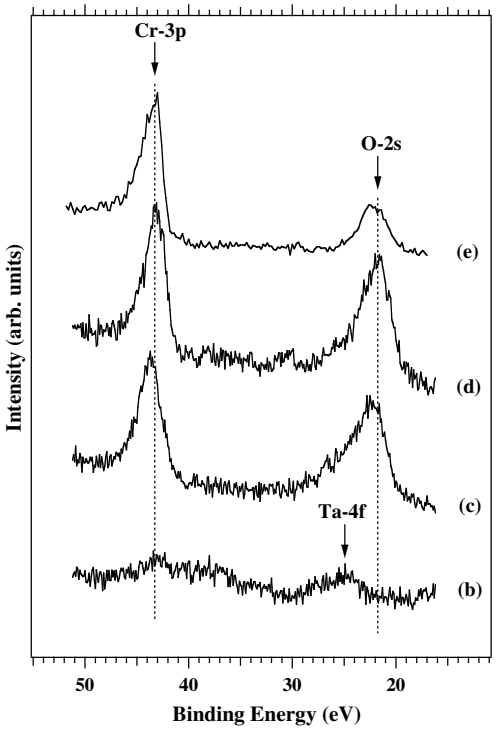

Figure 11. Cr 3p and O 2s core-electron spectra measured at $h\nu = 120$ eV and normal emission of (b) as-inserted $CrO_2(100)/TiO_2(100)$ sample, (c) sample sputtered for 10 min with 500 eV Ar ions, (d) sample annealed at $\sim$400 °C in 1×10^{-6} Torr O_2, and for comparison (e) $Cr_2O_3(0001)/Pt(111)$ measured at $h\nu = 155$ eV.

Table 4. Measured O 2s to Cr 3p core ratios and calculated surface stoichiometries.

Sample	H_O/H_{Cr}	N_O/N_{Cr}
$CrO_2(100)$, after sputter	0.83	2.1
$CrO_2(100)$, ∼400 °C anneal in O_2	0.85	2.2
$CrO_2(110)$, after sputter	0.69	1.8
$CrO_2(110)$, ∼200 °C anneal in O_2	0.71	1.8
$CrO_2(110)$, ∼400 °C anneal in O_2	0.78	2.0
$Cr_2O_3(0001)$	0.36	1.3

the appropriate photon energy, $N_O/N_{Cr} \approx (H_O/H_{Cr})\cdot(\sigma_{Cr}/\sigma_O)$. These values are presented in table 4.

The oxygen to chromium ratios calculated for the CrO_2 surfaces and the Cr_2O_3 surface are in reasonable agreement with the values expected for stoichiometric surfaces (2.0 and 1.5, respectively). Therefore, our data suggest that the majority of the surface region of each crystal is CrO_2 at all stages of the sample preparation. The implication of this is that neither the $CrO_2(110)$ nor the $CrO_2(100)$ surface is metallic.

Our UPS results seem to directly contradict the previously published theoretical results [1, 11–15] that predict that CrO_2 is a half-metallic ferromagnet. However, it must be emphasized that both UPS and LEED only probe the first 3 or 4 atomic layers of CrO_2, so our measurements reveal the electronic and geometric structure of the surface and near-surface regions of CrO_2. Therefore, a metal to semiconductor transition at the $CrO_2(110)$ and $CrO_2(100)$ surfaces may explain these contradictory results. Unfortunately, the few theoretical studies of the electronic structure of CrO_2 surfaces that have been published do not help clarify this situation [12, 60, 61]. A study of the effect of relaxation on the electronic properties of the $CrO_2(100)$ surface was performed by Hong and Che [60] using LSDA. Their calculations predict that the relaxed (100) surface remains in a half-metallic electronic state. Our UPS measurements of the $CrO_2(100)$ surface show no emission at E_F, which contradicts this theoretical prediction. The only other theoretical studies of the surface electronic structure of CrO_2 were performed for the (001) surface [12, 61]. Calculations by van Leuken and de Groot [12] using the localized spherical wave method predict that the density of states of the majority electrons crosses E_F at the (001) surface, retaining a half-metallic behaviour. On the other hand, calculations of the electronic structure of the relaxed $CrO_2(001)$ surface by Hong and Che [61] using LSDA + U find that a gap of about 1.2 eV is induced in the majority-spin density of states, resulting in a semiconducting, ferromagnetic surface. We know of no previous UPS studies of well-defined $CrO_2(001)$ surfaces, so it is not possible to verify this prediction of a semiconducting property for this termination.

In principle, the bulk electronic structure of CrO_2 could be experimentally determined with valence band photoemission by using relatively high photon energies. For instance, the mean free path of electrons with a kinetic energy of 500 eV is approximately twice that of electrons with a kinetic energy of 75 eV [62]. Therefore, valence band photoemission studies at a photon energy of 500 eV produce twice the probe depth of our UPS experiments. However, the typical instrumental resolution of synchrotron-based photoelectron spectroscopy is larger than 0.25 eV at a photon energy of 500 eV [34, 35]. Since we observe an onset of emission at about 0.2 eV below E_F, the previously published high photon energy valence band photoemission studies [52, 63] do not have sufficient instrumental resolution to distinguish between semiconducting and metallic behaviour at these surfaces.

Another aspect of these experiments that must be addressed is the shift in the valence and soft core emission features for the $CrO_2(100)$ surface after sputtering. To confirm the reproducibility of this behaviour, the experiments were repeated on a second set of samples

during a subsequent experimental run at CAMD several months after the initial measurements were made. These experiments reproduced the presence of a shift of the peak in the 3d states to higher binding energy for $CrO_2(100)$ and the lack of a shift for $CrO_2(110)$. This effect may be a result of surface stability. Since the (110) surface of TiO_2 is more stable than the (100) or (001) surfaces [55, 56], this may hold true for CrO_2, as well. Therefore, this shift to higher binding energies after sputtering may be due in part to changes in surface stoichiometry.

5. Conclusions

With the development of techniques to grow high-quality CrO_2 epitaxial films on TiO_2, it is possible to perform electronic structure measurements on well-defined surfaces of CrO_2. Our photoelectron spectroscopy measurements for both $CrO_2(110)$ and $CrO_2(100)$ show no emission at E_F, which indicates that neither surface is metallic. Although we cannot exclude the presence of Cr_2O_3 at these surfaces, analysis of the Cr 3p and O 2s soft-core peaks and LEED measurements, which show diffuse patterns with the correct symmetry for the (110) and (100) surfaces, provide evidence that stoichiometric CrO_2 is present at both surfaces. The most probable explanation for the lack of emission from the Fermi level is that the surface electronic structure of $CrO_2(110)$ and $CrO_2(100)$ differs from the bulk electronic structure. In other words, the formation of a surface may be causing a transition from metallic to semiconducting behaviour. However, a semi-metallic bulk electronic property for CrO_2 at room temperature could also explain our photoemission results.

Acknowledgments

This research was supported in part by the Louisiana Board of Regents Support Fund, the Petroleum Research Fund, the National Science Foundation, and the Department of Energy. The authors would like to thank the staff of CAMD for their technical support. The NSLS is supported by the Divisions of Materials and Chemical Sciences of the US Department of Energy.

References

[1] Schwarz K 1986 *J. Phys. F: Met. Phys.* **16** L211
[2] de Groot R A, Mueller F M, van Engen P G and Buschow K H J 1983 *Phys. Rev. Lett.* **50** 2024
[3] Coey J M D and Venkatesan M 2002 *J. Appl. Phys.* **91** 8345
[4] Coey J M D, Versluijs J J and Venkatesan M 2002 *J. Phys. D: Appl. Phys.* **35** 2457
[5] Mazin I I 1999 *Phys. Rev. Lett.* **83** 1427
[6] Tedrow P M and Meservey R 1994 *Phys. Rep.* **238** 173
[7] Yanese A and Siratori K 1984 *J. Phys. Soc. Japan* **53** 312
[8] Coey J M D, Viret M and Ranno L 1995 *Phys. Rev. Lett.* **75** 3910
[9] Kobayashi K I, Kimura T, Sawada H, Terakura K and Tokura Y 1998 *Nature* **395** 677
[10] Kouvel J S and Rodbell D S 1967 *J. Appl. Phys.* **38** 979
[11] Robbert P S, Geisler H, Ventrice C A Jr, van Ek J, Chaturvedi S, Rodriguez J A, Kuhn M and Diebold U 1998 *J. Vac. Sci. Technol.* A **16** 990
[12] van Leuken H and de Groot R A 1995 *Phys. Rev.* B **51** 7176
[13] Korotin M A, Anisimov V I, Khomskii D I and Sawatzky G A 1998 *Phys. Rev. Lett.* **80** 4305
[14] Stagarescu C B, Su X, Eastman D E, Altmann K N, Himpsel F J and Gupta A 2000 *Phys. Rev.* B **61** R9233
[15] Craco L, Laad M S and Müller-Hartmann E 2003 *Phys. Rev. Lett.* **90** 237203
[16] Baibich M N, Broto J M, Fert A, Van Dau N, Petroff F, Eitenne P, Creuzet G, Friederich A and Chazelas J 1988 *Phys. Rev. Lett.* **61** 2472
[17] Tanaka C T, Nowak J and Moodera J S 1999 *J. Appl. Phys.* **86** 6239
[18] van der Zaag P J, Bloemen P J H, Gaines J M, Wolf R M, van der Heijden P A A, van de Veerdonk R J M and de Jonge W J M 2000 *J. Magn. Magn. Mater.* **211** 301

[19] Gupta A, Li X W and Xiao G 2001 *Appl. Phys. Lett.* **78** 1894
[20] Kim W, Kawaguchi K and Koshizaki N 2003 *J. Appl. Phys.* **93** 8032
[21] Parker J S, Ivanov P G, Lind D M and Xiong P 2004 *Phys. Rev.* B **69** R220413
[22] Miao G X, LeClair P, Gupta A, Xiao G, Varela M and Pennycook S 2006 *Appl. Phys. Lett.* **89** 022511
[23] Jullière M 1975 *Phys. Lett.* A **54** 225
[24] LeClair P, Swagten H J M and Moodera J S 2005 *Ultrathin Magnetic Structures III: Fundamentals of Nanomagnetism* ed J A C Bland and B Heinrich (Berlin: Springer) p 51
[25] Caballero J A, Park Y D, Childress J R, Bass J, Chiang W-C, Reilly A C, Pratt W P Jr and Petroff F 1998 *J. Vac. Sci. Technol.* A **16** 1801
[26] Li X W, Gupta A, Xiao G, Qian W and Dravid V P 1998 *Appl. Phys. Lett.* **73** 3282
[27] Miao G X, Gupta A, Sims H, Butler W H, Ghosh S and Xiao G 2005 *J. Appl. Phys.* **97** 10C924
[28] Chamberland B L 1977 *CRC Crit. Rev. Solid State Mater. Sci.* **7** 1
[29] Dai J, Tang J, Xu H, Spinu L, Wang W, Wang K, Kumbhar A, Li M and Diebold U 2000 *Appl. Phys. Lett.* **77** 2840
[30] Cheng R, Xu B, Borca C N, Sokolov A, Yang C-S, Yuan L, Liou S-H, Doudin B and Dowben P A 2001 *Appl. Phys. Lett.* **79** 3122
[31] Cheng R, Komesu T, Jeong H K, Yuan L, Liou S H, Doudin B, Dowben P A and Losovyj Y B 2002 *Phys. Lett.* A **302** 211
[32] Cheng R, Caruso A N, Yuan L, Liou S-H and Dowben P A 2003 *Appl. Phys. Lett.* **82** 1443
[33] Zheng R K, Liu H, Wang Y and Zhang X X 2004 *Appl. Phys. Lett.* **84** 702
[34] Hüfner S 1996 *Photoelectron Spectroscopy* 2nd edn (Berlin: Springer)
[35] Ertl G and Küppers J 1974 *Low Energy Electrons and Surface Chemistry* (Weinheim: Verlag Chemie)
[36] Kittel C 1996 *Introduction to Solid State Physics* 7th edn (New York: Wiley) pp 159–62
[37] Ashcroft N W and Mermin N D 1976 *Solid State Physics* (Fort Worth: Saunders College Publication) pp 284–311
[38] Ranno L, Barry A and Coey J M D 1997 *J. Appl. Phys.* **81** 5774
[39] Li X W, Gupta A, McQuire T R, Duncombe P R and Xiao G 1999 *J. Appl. Phys.* **85** 5585
[40] Stampe P A, Kennedy R J, Watts S M and von Molnár S 2001 *J. Appl. Phys.* **89** 7696
[41] DeSisto W J, Broussard P R, Ambrose T F, Nadgorny B E and Osofsky M S 2000 *Appl. Phys. Lett.* **76** 3789
[42] Anguelouch A, Gupta A, Xiao G, Abraham D W, Ji Y, Ingvarsson S and Chien C L 2001 *Phys. Rev.* B **64** R180408
[43] Watts S M, Wirth S, von Molnár S, Barry A and Coey J M D 2000 *Phys. Rev.* B **61** 9621
[44] Gupta A, Li X W and Xiao G 2000 *J. Appl. Phys.* **87** 6073
[45] Ashcroft N W and Mermin N D 1976 *Solid State Physics* (Fort Worth: Saunders College Publication) p 8
[46] Soulen R J Jr, Byers J M, Osofsky M S, Nadgorny B, Ambrose T, Cheng S F, Broussard P R, Tanaka C T, Nowak J, Moodera J S, Barry A and Coey J M D 1998 *Science* **282** 85
[47] Huang D J, Wu W P, Chen J, Chang C D F, Chung S C, Yuri M, Lin H J, Johnson P D and Chen C T 2002 *Rev. Sci. Instrum.* **73** 3778
[48] Kiss T, Kanetaka F, Yokoya T, Shimojima T, Kanai K, Shin S, Onuki Y, Togashi T, Zhang C, Chen C T and Watanabe S 2005 *Phys. Rev. Lett.* **94** 057001
[49] Kämper K P, Schmitt W, Güntherodt G, Gambino R J and Ruf R 1987 *Phys. Rev. Lett.* **59** 2788
[50] Dedkov Y S, Fonine M, König C, Rüdiger U, Güntherodt G, Senz S and Hesse D 2002 *Appl. Phys. Lett.* **80** 4181
[51] Tsujioka T, Mizokawa T, Okamoto J, Fujimori A, Nohara M, Takagi H, Yamaura K and Takano M 1997 *Phys. Rev.* B **56** R15509
[52] Dedkov Y S, Vinogradov A S, Fonin M, König C, Vyalikh D V, Preobrajenski A B, Krasnikov S A, Kleimenov E Y, Nesterov M A, Rüdiger U, Molodtsov S L and Güntherodt G 2005 *Phys. Rev.* B **72** 060401
[53] Strehlow W H and Cook E L 1973 *J. Phys. Chem. Ref. Data* **2** 163
[54] Wyckoff R W G 1960 *Crystal Structures* (New York: Interscience)
[55] Henrich V E and Cox P A 1994 *The Surface Science of Metal Oxides* (Cambridge: Cambridge University Press)
[56] Diebold U 2003 *Surf. Sci. Rep.* **48** 53
[57] Dowben P A, LaGraffe D and Onellion M 1989 *J. Phys.: Condens. Matter* **1** 6571
[58] Ventrice C A Jr, Ehrlich D, Garfunkel E L, Dillmann B, Heskett D and Freund H-J 1992 *Phys. Rev.* B **46** 12892
[59] Yeh J J and Lindau I 1985 *At. Data Nucl. Data Tables* **32** 1
[60] Hong F and Che J G 2006 *Appl. Phys. Lett.* **88** 121903
[61] Hong F and Che J G 2006 *Phys. Rev. Lett.* **96** 167206
[62] Penn D R 1987 *Phys. Rev.* B **35** 482
[63] Chang C F, Huang D J, Tanaka A, Guo G Y, Chung S C, Kao S-T, Shyu S G and Chen C T 2005 *Phys. Rev.* B **71** 052407